Multi-vortex states in magnetic nanoparticles

W. L. Gan, M. Chandra Sekhar, D. W. Wong, I. Purnama, S. Y. Chiam, L. M. Wong, and W. S. Lew

Citation: Applied Physics Letters **105**, 152405 (2014); doi: 10.1063/1.4898349
View online: http://dx.doi.org/10.1063/1.4898349
View Table of Contents: http://scitation.aip.org/content/aip/journal/apl/105/15?ver=pdfcov
Published by the AIP Publishing

Multi-vortex states in magnetic nanoparticles

W. L. Gan,[1] M. Chandra Sekhar,[1] D. W. Wong,[1] I. Purnama,[1] S. Y. Chiam,[2] L. M. Wong,[2] and W. S. Lew[1,a)]
[1]*School of Physical and Mathematical Sciences, Nanyang Technological University, 21 Nanyang Link, Singapore 637371*
[2]*Institute of Materials Research and Engineering, A*STAR (Agency for Science, Technology and Research), 3 Research Link, Singapore 117602*

(Received 17 July 2014; accepted 5 October 2014; published online 15 October 2014)

We demonstrate a fabrication technique to create cylindrical NiFe magnetic nanoparticles (MNPs) with controlled dimensions and composition. MNPs thicker than 200 nm can form a double vortex configuration, which consists of a pair of vortices with opposite chirality. When MNPs thicker than 300 nm are relaxed after saturation, it forms a frustrated triple vortex state which produces a higher net magnetization as verified by light transmissivity measurements. Therefore, a greater magnetic torque can be actuated on a MNP in the triple vortex state. © *2014 AIP Publishing LLC*.
[http://dx.doi.org/10.1063/1.4898349]

Magnetic particles have steadily gained interest in clinical applications due to their unique properties which allow them to function at the cellular and molecular level of biological interactions.[1,2] A key advantage of the magnetic particles have over their nonmagnetic counterparts is the ability to actuate a magnetic force remotely under an externally applied magnetic field. Utilizing "nanosurgeons," where magnetic nanoparticles (MNPs) with a high magnetic dipole moment are used, researchers have demonstrated surgical removal of targeted cells.[3] Magnetic particles can also be highly specific. For instance, researchers have used magnetic beads to selectively activate the TREK-1 mechanosensitive ion channel.[4,5] In yet another step closer to clinical applications, biofunctionalized NiFe microdiscs have been used to demonstrate targeted magnetomechanical cancer cell destruction with the application of small-amplitude and low-frequency alternating magnetic field.[6] The resulting magnetic torque acting on the microdisc generates an oscillatory motion that transmits a mechanical force to the cell membrane. Nano-sized magnetic particles have also been used for other clinical applications such as magnetic resonance imaging, magnetic targeted drug delivery, and magnetic hyperthermia.[7–10] The advantage of these methods over the conventional cancer therapy is the localization of treatment of the cancerous tumor, which minimizes harmful side effects to the patient.

In this letter, we demonstrate a MNP fabrication method which combines compositionally modulated nanowire growth and chemical slicing to create NiFe MNP with multiple vortex states. While magnetization dynamics in nanodisks and cylindrical nanowires have been well studied,[11–14] there is a lack of discussion on cylindrical MNPs in the intermediate length of 200 nm to 1 μm. Here, we show that it is possible to form a triple vortex or a double vortex magnetization configuration in the NiFe MNPs depending on their aspect ratio. The transition between vortex states during the reversal process in the presence of perpendicular magnetic fields is also reported. Owing to the unique properties of the multi-vortex states, we show that our MNP fabrication method is versatile and may be potentially useful for magnetomechanical cell destruction and other torque-based biomedical applications.[4,6]

First, compositionally modulated NiFe nanowires are grown using the template-assisted electrodeposition technique. The chosen growth template was the Whatman Anodisc 13 anodized aluminum oxide (AAO) membrane with a pore diameter of 350 nm as measured using a Scanning Electron Microscope (SEM). A 400 nm seed layer of aluminum was deposited on one side of the AAO template via thermal evaporation. Figure 1(a) shows the schematic of the electrodeposition setup. The electrolyte consists of 0.5M nickel sulphate, 0.01M iron sulphate, and 0.5M boric acid. To create the compositional modulations, alternating pulses of high potential ($V_H = -1.45$ V) and low potential ($V_L = -0.95$ V) were applied during the deposition process. Due to the anomalous codeposition effect of Fe group metals, the less noble metal (Fe) is deposited preferentially when the applied potential is low. However, when the applied potential is increased, the electrodeposition enters the diffusion limited regime where the deposited alloy has a composition similar to the ion concentration in the electrolyte. Since there are more Ni^{2+} ions than Fe^{2+} ions, a nickel-rich layer is formed within the AAO membrane when V_H is applied, while an iron-rich layer is formed when V_L is applied.[15] By alternating the potential between V_H and V_L, compositionally modulated nanowires will then be formed within the AAO membrane.

Subsequently, the compositionally modulated nanowires were released by dissolving the AAO template and the aluminum layer in sodium hydroxide solution. SEM images of the released nanowires are shown at the bottom of Figure 1(b). The nanowires were then thoroughly rinsed with deionized water to be dealkalized. In the third step, the nanowires were etched with 0.67% dilute nitric acid. The SEM image in Figure 1(c) shows the compositionally modulated nanowires which have undergone partial chemical etching. The observed constrictions along the length are due to the

a)Author to whom correspondence should be addressed. Electronic mail: wensiang@ntu.edu.sg.

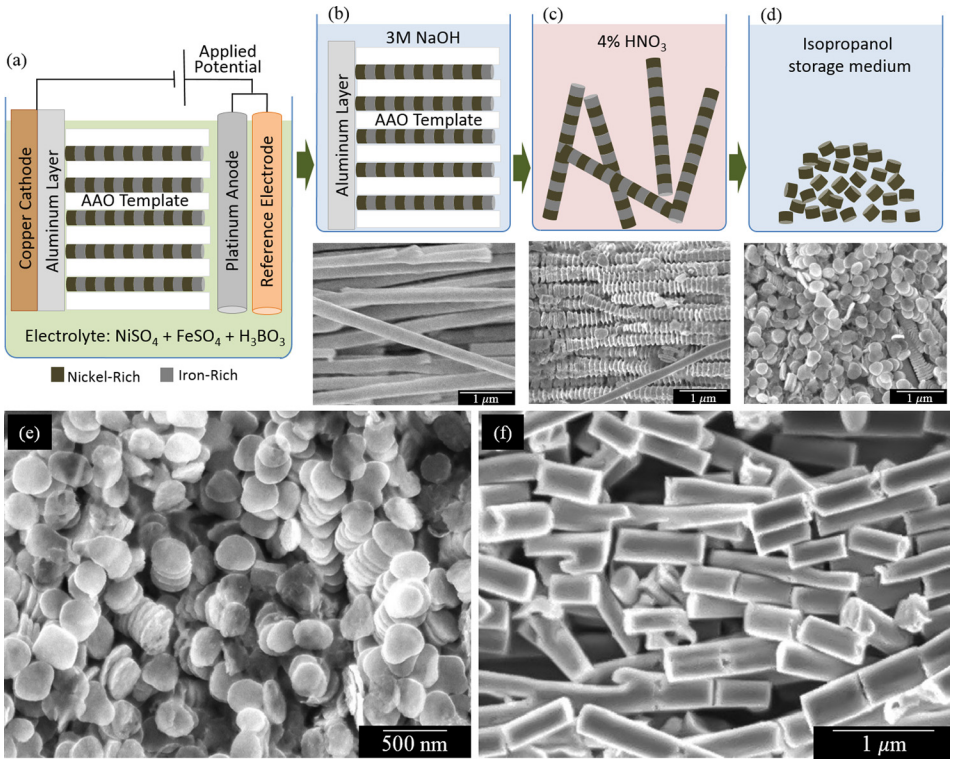

FIG. 1. (a) Schematic diagram of the three electrode electrodeposition setup. (b) Schematic of compositionally modulated NiFe nanowires by varying the potential during deposition. Shown below is the SEM image of the nanowires grown (c) partially etched nanowires in 0.67% dilute nitric acid. (d) Nanowire segments with lower etching rate are sliced as MNP after complete etching. (e) and (f) NiFe MNP of thicknesses 70 nm and 600 nm, respectively.

differential etching rate between the different (compositional) layers of the NiFe nanowires. The diameter of the constrictions will decrease with further etching until only the nickel-rich layers remain as the desired final product—the NiFe MNPs, as shown in Figure 1(d). Finally, the solution is filtered through an Acrodisc syringe filter with pore size of 800 nm and the MNPs are recovered as the filtrate.

One of the advantages of this fabrication method is the easy control over the thickness of the MNP via altering the duration of the high potential pulses V_H. MNPs with thicknesses of 70 and 600 nm were fabricated with V_H pulse duration of 2 and 50 s as shown in Figures 1(e) and 1(f). An increase in the V_H pulse duration results in an increased MNP thickness. The fabrication method is also capable of producing MNPs composed of different Ni and Fe ratios. By changing either the electrodeposition potential or the concentration of metal ions in the electrolyte, the MNP composition can be customized. The EDX spectrum of our fabricated MNPs reveals that elemental compositions of $Ni_{88}Fe_{12}$, $Ni_{76}Fe_{24}$, $Ni_{52}Fe_{48}$, and $Ni_{36}Fe_{64}$ MNPs can be achieved.[25] Selective Area Diffraction Pattern (SAED) imaging of an MNP indicates a polycrystalline structure.

The magnetization configurations and switching process of cylindrical MNPs with a diameter of 350 nm under applied magnetic fields were then studied by using micromagnetic simulations. Object oriented micromagnetic framework (OOMMF) software was used to perform the micromagnetic simulations.[16] The material parameters are used for permalloy; saturation magnetization $(M_s) = 860 \times 10^3$ A/m, exchange stiffness constant $(A_{ex}) = 1.3 \times 10^{-11}$ J/m, and magnetocrystalline anisotropy $k = 0$. The damping constant (α) is fixed to be 0.01. In soft magnetic materials such as NiFe, the final magnetization configuration is influenced mainly by the shape anisotropy and exchange interaction.[17] Therefore, in MNPs with thickness below 200 nm, where the shape anisotropy dominates, the magnetization tends to form a vortex structure with minimal out of plane component.[13,14]

The simulations show that the MNPs have a few different switching processes with respect to an out of plane field depending on their thickness. Figure 2(a) shows the hysteresis loop for a MNP of thickness 200 nm. The MNP of interest was first saturated by an out-of-plane applied magnetic field (H_{app}) and then relaxed. The magnetization in the 200 nm MNP relax by gradually curling in opposite chirality at each end. This results in a double vortex structure where the vortex at each end of the MNP has opposite chirality. The two vortices are connected at the center of the MNP where the magnetization is aligned along the cylindrical axis as highlighted in the top left inset of Figure 2(a). As H_{app} is lowered below a threshold field of 190 mT, the magnetization collapses into a single vortex state as shown in the bottom right of Figure 2(a). The rapid switch between the single and the double vortex configuration results in an abrupt drop along the hysteresis loop of the 200 nm MNP as shown in Figure 2(a).

For MNPs thicker than 300 nm, the magnetization initially forms a double vortex state as H_{app} is decreased. However, as the magnetic field continues to decrease, the Zeeman energy sustaining the uniform alignment of the magnetization at the center of the two vortices is decreased. Unlike the 200 nm MNPs where little energy is required to switch the chirality of one of the vortices and reverts into the single vortex state, the magnetization in the thicker 300 nm MNPs is instead forced to form a frustrated triple vortex state. As seen from Figure 2(b), the triple-vortex state appears similar to a double vortex state at first glance, with two vortices of opposite chirality residing at each end of the MNP (ii) and (iii). However, a closer inspection reveals that another magnetic vortex resides on the curved surface of the MNP (iv). The additional magnetic vortex permeates through

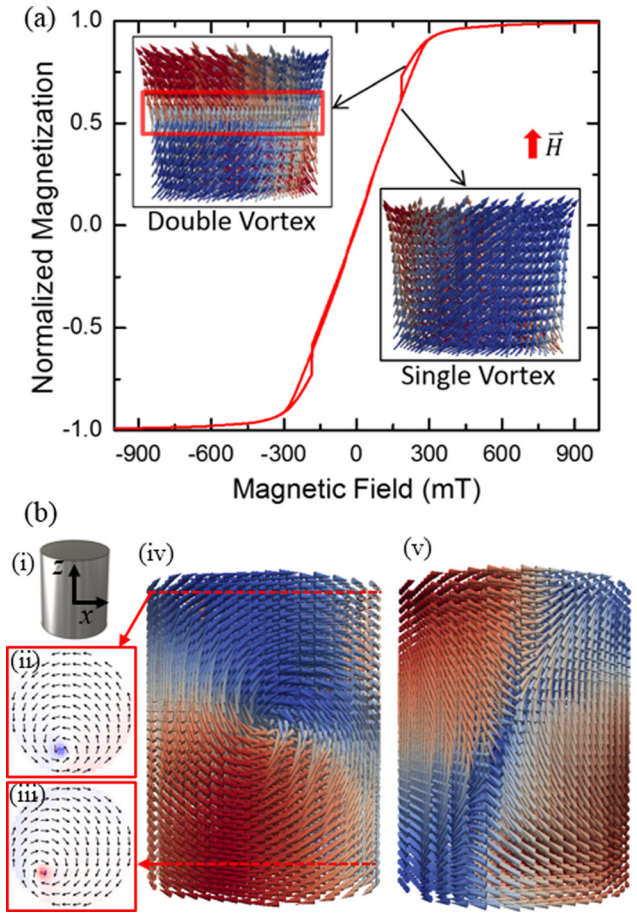

FIG. 2. (a) The hysteresis curve of a 200 nm thick MNP. The 3D glyphs represent the magnetization vectors with its color representing the in-plane direction. (b) The magnetization structure of a MNP in triple vortex state. (i) Schematic representation of the MNP orientations in Cartesian coordinates. (ii) and (iii) The cross-sectional view of the MNP magnetization at the top and bottom as seen from the $-z$ direction. Pixel colors show the out of plane magnetization component. (iv) The front view of the MNP magnetization with the middle vortex facing out of the paper as seen from x direction. (v) MNP magnetization as seen from the $-x$ direction.

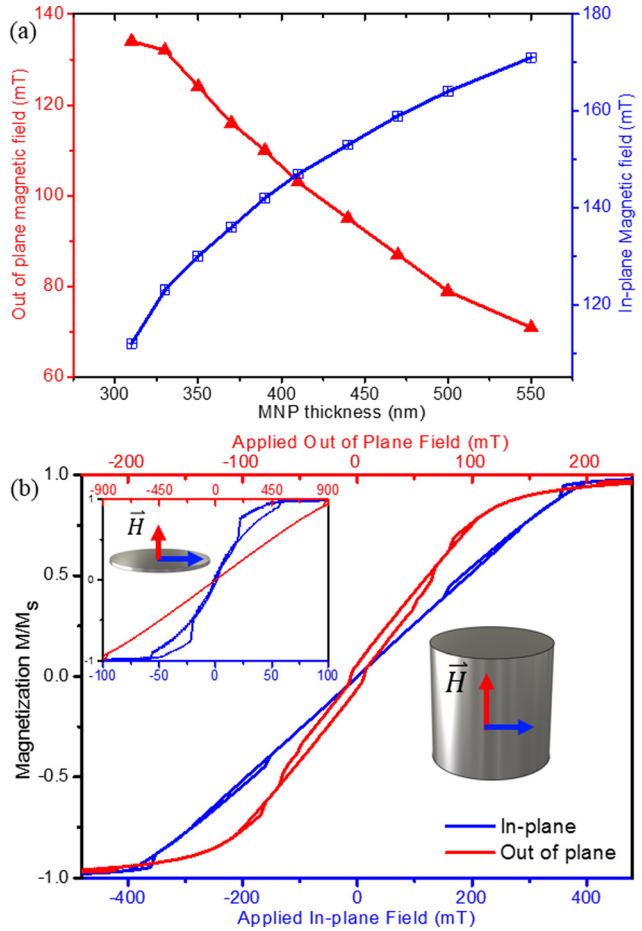

FIG. 3. (a) The threshold field strength required to eliminate the triple vortex configuration as a function of MNP thickness. (b) The hysteresis curve of a 500 nm thick MNP in both directions. The saturation occurs at 200 and 450 mT for the easy and hard axes, respectively. Top left inset shows the hysteresis curve of 1 μm diameter and 60 nm thick MNP with the easy axis being the in-plane direction.

the diameter of the MNP and disappears on the other side (v). Although Bloch, vortex, and helical domain walls are known to exist in cylindrical nanowires,[18–20] it is surprising to observe an additional vortex core forming in such a low aspect ratio MNP. The triple vortex state was also found to be stable in ferromagnetic materials over a wide range of material parameters.[25]

Consequently, the stability of triple vortex magnetization configuration with respect to MNP thickness was studied by subjecting the MNP to a gradually increasing H_{app} until the triple vortex state is annihilated. As shown in Figure 3(a), for increased thickness of MNP, the threshold value for in-plane field increases, whereas the threshold value for perpendicular field decreases. Using shape anisotropy arguments, the triple vortex state in thicker MNPs is expected to have a higher tolerance to in-plane H_{app} while being more susceptible to perpendicular H_{app}. Figure 3(b) shows the hysteresis curve for a 500 nm thick MNP in both the in-plane and out of plane directions. When applying an in-plane field to a MNP in the triple vortex state, we found that one of the vortices at the ends is abruptly annihilated at a threshold field, while the other remaining vortex typically requires another 100 mT to annihilate, resulting in a saturated state for the MNP. Applying an out of plane field to the MNP in triple vortex state, the magnetic vortex residing at the curve surface of the MNP is first annihilated at a threshold field of 70 mT, forming a double vortex configuration. Further increasing the field causes the two vortices to uncurl along the cylinder axis and subsequently achieving saturation.

For comparison, the microdisks studied in magnetomechanical cell destruction has an easy axis in the in-plane direction.[6] However, due to the symmetry of cylinders, all directions along the plane of the microdisk are degenerate. Therefore, such microdisks can only experience a magnetic torque along 2 rotational axes. In contrast, our fabricated MNPs have only 1 easy axis which allows the MNPs to rotate in any direction to align with H_{app}. The experimental hysteresis curve of our fabricated 500 nm thick MNP is qualitatively similar to the simulated curve and confirms that the easy axis lies along the cylinder axis.[25] The magnetic torque τ acting on a MNP can be approximated by $\tau = m \times \mu_0 H$. Applying a 1 mT magnetic field at an angle of 45° to a 500 nm MNP in triple vortex state, we obtain the resulting force F at the edge of the MNP to be 2 pN. While physically rupturing a cell membrane typically requires at least hundreds of pN, it has been shown that even ~0.5 pN can

activate ion channels which may accelerate cell apoptosis.[21–23] Therefore, the fabricated MNPs can potentially be used for magnetomechanical cell destruction. Although it has been shown that synthetic antiferromagnets (SAFs) can produce magnetic moments of up to an order of magnitude more than the vortex particles studied, the SAFs have a high susceptibility and thus increased self-polarization and agglomeration.[24] On the other hand, our fabricated vortex-based MNPs have a much lower susceptibility than required for the formation of particle chains and single domains in the absence of H_{app}.[24] The effects of dipolar interactions on the magnetization of MNPs are presented in the supplementary material.[25]

The magnetic torque acting on MNPs can be experimentally observed by studying the light transmissivity dynamics of a suspension of MNPs. When H_{app} is applied to a suspension of MNPs, the induced torque aligns the net magnetic moments of the MNPs to H_{app}. This alignment causes the light transmissivity of the MNP suspension to increase abruptly. In our experiment, a quadrupole electromagnet is used to create a H_{app} which alternates between two orthogonal directions, while a laser and a photodiode measure the transmitted laser intensity along one direction. Before the experiment was conducted, the MNP suspension was exposed to a 1 T uniform magnetic field and relaxed to reset the MNP magnetization states. The intensity of a laser beam transmitted through a suspension of 400 nm MNP under the influence of a 0.9 mT alternating magnetic field was measured against time. The change in transmitted laser intensity over a period ΔI is taken as $\Delta I = I_{max} - I_{min}$, where I_{max} and I_{min} are the maximum and minimum laser intensity measured over a period.

In Figure 4, the frequency response of ΔI is shown for MNPs of thickness 250 and 400 nm with their ΔI values at 1 Hz taken to be 100%. The decrease in the intensity oscillation amplitude with increasing frequency is a result of the lack of time for complete alignment to the H_{app}. As expected, the thicker 400 nm capable of forming the triple vortex state saturates much faster than the 250 nm MNPs. At the same ΔI value, the corresponding frequency of the 400 nm MNPs is generally double of the 250 nm MNPs. Therefore, the 400 nm MNP is able to rotate about twice as fast as a 250 nm MNP under the same H_{app}, despite the 400 nm MNPs having a moment of inertia 2.61 times more.

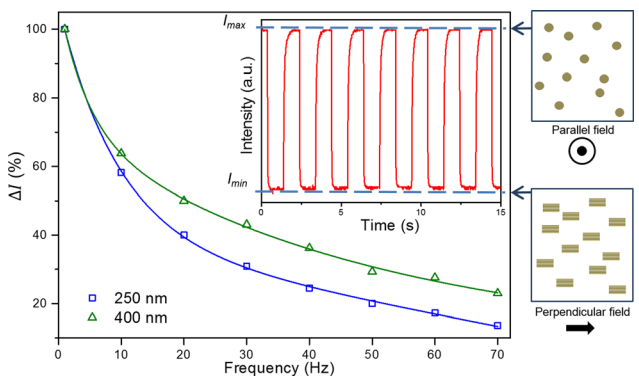

FIG. 4. The change in intensity ΔI of a laser beam transmitted through a MNP colloidal suspension as a function of applied field frequency. ΔI is the average difference between I_{max} and I_{min} at the corresponding field frequency.

The light transmissivity measurements verify that the thicker MNPs capable of forming the triple vortex state can indeed produce a higher magnetic torque.

In summary, a technique to fabricate NiFe MNPs of different dimensions was demonstrated using a combination of pulsed electrodeposition and differential etching. A good control over MNP composition was achieved by modifying electrolyte composition and deposition potential. Although the scope of the study was limited to NiFe alloys, it is theoretically possible to create MNPs composed of other metallic alloys as long as their ions have different reduction potentials. The fabrication technique can also create high aspect ratio MNPs not achievable by the lithographic processes commonly employed to grow cylindrical MNPs. Micromagnetic simulations have shown that as the thickness of the MNP increases, it is possible to form double and triple vortex configurations. Despite being at a substantially higher energy state as compared to a single vortex state, the triple vortex state was found to be stable at remanence. By measuring the relationship between the applied magnetic field and light transmissivity of a MNP suspension, we have concluded that MNPs in triple vortex state indeed have a net magnetization stronger than a MNP in single vortex state. A key advantage provided by the triple vortex configuration is the increase in magnetization at remanence, which is useful for magnetic torque based biomedical applications.[4,6]

This work was supported by the Singapore National Research Foundation CRP grant (Non-volatile memory and logic integrated circuit devices, NRF-CRP009-2011-01). We also wish to acknowledge the funding for this project from Nanyang Technological University under the Undergraduate Research Experience on CAmpus (URECA) programme.

[1]C. C. Berry and A. S. G. Curtis, J. Phys. D: Appl. Phys. **36**, R198 (2003).
[2]Y. Pan, X. Du, F. Zhao, and B. Xu, Chem. Soc. Rev. **41**, 2912–2942 (2012).
[3]B. G. Nair, Y. Nagaoka, H. Morimoto, Y. Yoshida, T. Maekawa, and D. S. Kumar, Nanotechnology **21**, 455102 (2010).
[4]J. Dobson, Nat. Nanotechnol. **3**, 139–143 (2008).
[5]S. Hughes, S. McBain, J. Dobson, and A. J. El Haj, J. R. Soc. Interface **5**, 855–863 (2008).
[6]D. H. Kim, E. A. Rozhkova, I. V. Ulasov, S. D. Bader, T. Rajh, M. S. Lesniak, and V. Novosad, Nat. Mater. **9**, 165–171 (2010).
[7]O. Veiseh, J. Gunn, and M. Zhang, Adv. Drug Delivery Rev. **62**, 284–304 (2010).
[8]B. Thiesen and A. Jordan, Int. J. Hyperthermia **24**, 467–474 (2008).
[9]V. I. Shubayev, T. R. Pisanic II, and S. Jin, Adv. Drug Delivery Rev. **61**, 467–477 (2009).
[10]J. Chomoucka, J. Drbohlavova, D. Huska, V. Adam, R. Kizek, and J. Hubalek, Pharmacol. Res. **62**, 144–149 (2010).
[11]E. R. Evarts, R. Heindl, W. H. Rippard, and M. R. Pufall, Appl. Phys. Lett. **104**, 212402 (2014).
[12]R. Pulwey, M. Rahm, J. Biberger, and D. Weiss, IEEE Trans. Magn. **37**, 2076–2078 (2001).
[13]Q. F. Xiao, J. Rudge, B. C. Choi, Y. K. Hong, and G. Donohoe, Appl. Phys. Lett. **89**, 262507 (2006).
[14]R. Ferre, K. Ounadjela, J. M. George, L. Piraux, and S. Dubois, Phys. Rev. B **56**, 14066 (1997).
[15]Á. Llavona, L. Pérez, M. C. Sánchez, and V. de Manuel, Electrochim. Acta **106**, 392–397 (2013).
[16]M. J. Donahue and D. G. Porter, Interagency Report No. NISTIR 6376, National Institute of Standard and Technology, Gaithersburg, MD, 1999.
[17]D. Betto and J. M. D. Coey, J. Appl. Phys. **115**, 17D138 (2014).
[18]H. G. Piao, J. H. Shim, D. Djuhana, and D. H. Kim, Appl. Phys. Lett. **102**, 112405 (2013).

[19]J. A. Otálora, J. A. Lopez-Lopez, P. Vargas, and P. Landeros, Appl. Phys. Lett. **100**, 072407 (2012).
[20]M. C. Sekhar, H. F. Liew, I. Purnama, W. S. Lew, M. Tran, and G. C. Han, Appl. Phys. Lett. **101**, 152406 (2012).
[21]A. Stutzin and E. K. Hoffmann, Acta Physiol. **187**, 27–42 (2006).
[22]F. Lang, M. Föller, K. S. Lang, P. A. Lang, M. Ritter, E. Gulbins, and S. M. Huber, J. Membr. Biol. **205**, 147–157 (2005).
[23]B. Martinac, J. Cell Sci. **117**, 2449–2460 (2004).
[24]S. Leulmi, H. Joisten, T. Dietsch, C. Iss, M. Morcrette, S. Auffret, P. Sabon, and B. Dieny, Appl. Phys. Lett. **103**, 132412 (2013).
[25]See supplemental material at http://dx.doi.org/10.1063/1.4898349 for the elementary characterization of fabricated MNPs, magnetization phase of MNP, experimental hysteresis curve of 500 nm thick MNPs, and the effect of dipolar interactions on magnetization configuration.